Received: 20 June 2022 | Revised: 8 October 2022 | Accepted: 29 October 2022

DOI: 10.1002/eqe.3773

RESEARCH ARTICLE

WILEY

Effect of modeling of inherent damping on the response and collapse performance of seismically isolated buildings

Shoma Kitayama[1] | **Michael C. Constantinou**[2]

[1]School of Civil Engineering, University of Leeds, Leeds, UK

[2]Department of Civil, Structural and Environmental Engineering, University at Buffalo, State University of New York, Buffalo, New York, USA

Correspondence
Shoma Kitayama, School of Civil Engineering, University of Leeds, Leeds, LS2 9JT, UK.
Email: s.kitayama@leeds.ac.uk

Abstract

This paper investigates the effect of inherent damping modeling on the computed seismic response and collapse performance of selected seismically isolated buildings. The analyzed seismically isolated buildings were designed by the procedures of the ASCE/SEI 7–16 standard. The structure is a six-story perimeter frame building designed with special moment resisting frames or with special concentrically braced frames (SCBF) for a location in California. Three different seismic isolation systems are considered: (i) triple friction pendulum (TFP) bearings without moat walls, (ii) TFP bearings with moat walls (double concave [DC] friction pendulum bearings with moat walls have effectively the same ultimate behavior), and (iii) DC friction pendulum bearings without moat wall. The superstructure inherent damping schemes considered are (i) zero damping, (ii) modal damping, (iii) Zareian-Medina damping, (iv) added virtual viscous dampers with and without force-caps, and (v) added virtual viscous dampers with the same damping constant value. The response parameters computed are peak floor accelerations, peak story drift ratios, peak residual story drift ratios, peak isolator horizontal displacement, and floor acceleration spectra. Also, the probability of collapse in the maximum considered earthquake (MCE_R) is computed. It is shown that the modeling approach for the inherent damping has minor effects on the computed responses and the collapse probability of the studied seismically isolated buildings, except for the peak floor acceleration and the floor response spectra for periods below one second. It is suggested that a convenient way to model inherent damping is to use virtual viscous dampers with all having the same damping constant.

KEYWORDS

ASCE/SEI 7–16 standard, conditional spectra, inherent damping, seismic isolation, seismic performance assessment, viscous damping

1 | INTRODUCTION

Nonlinear response history analysis is needed for performance-based seismic design and assessment of buildings.[1] By using properly scaled records of earthquake acceleration time histories on the ground, nonlinear response history analysis computes a structural response that is consistent with the expected seismic demand at the site.[2] While tools for performing nonlinear response history analysis have been developed and their use by design professionals has been encouraged,[3] the procedure requires a large degree of engineering judgment compared with other simplified procedures, such as the Equivalent Lateral Force and Response Spectrum procedures.[4] As a result, the design and analysis processes require assumptions, including nonlinear inelastic modeling of structures. It has been known that the structural models used in the analysis affect the results of the design and assessment.[5]

One of the assumptions made by analysts is on modeling the inherent ability of structural systems to dissipate energy while responding elastically at the global level. This ability is traditionally referred to as inherent damping and results from a variety of mechanisms including internal material friction, hysteresis in non-structural elements, friction between structural and nonstructural elements, and radiation into the soil or surrounding fluid, etc.[6,7] These energy dissipation mechanisms in real structures are complex and difficult to accurately model. Thus, in practice, energy dissipation not associated with structural inelastic action (which relates to damage) is typically accounted for by using viscous damping models.[8]

Recent research led to some degrees of agreement as to how to model inherent damping for seismically isolated buildings. One recommendation made was not to use mass-proportional damping. This is because using mass-proportional damping results in unintended significant reduction of displacements as if viscous dampers existed between the building and the ground.[9–11] Another recommendation for modeling inherent damping for seismically isolated building is to use zero-percent damping for the "purely isolated modes" (Figure 1) and constant non-zero damping values (e.g., 2% for steel structures) for the higher modes.[12–14] This is for minimizing the introduction of unintended damping in the isolation system during construction of the global damping matrix (the so-called "damping leakage" or "spurious damping" problem). The introduction of unintended damping in the isolation system is an important issue as for construction of the global damping matrix, nonlinear elements in the isolation system are represented by equivalent elastic properties. While the global damping matrix remains constant during response history analysis, the elements in the isolation system undergo inelastic action that results in reduction of their effective stiffness and an unintended magnification of damping. While this problem exists for all structures with elements that undergo inelastic action, it is particularly acute for seismically isolated ones due to the large effective ductility ratio in the seismic isolation system as discussed in Hall,[15] Sarlis and Constantinou[12] and Chopra and McKenna.[16] For example, consider that the isolation system has elastoplastic behavior with a yield displacement Y (Y~1 mm or less for a sliding isolation system) and yield strength F_Y (Figure 2). The inherent damping ratio is specified as β (say 2% of critical) in each mode of vibration and the elastic stiffness k_{el} ($= F_Y/Y$) is used in the construction of the inherent global damping matrix. Consider the isolation system displacement reaching a value of D, for which the effective stiffness (secant stiffness) k_s is F_Y/D. The damping ratio β is expressed as $\beta = C/\sqrt{(4mk)}$, where C is the damping constant, m is the mass and k is the stiffness of isolation system. When the value of stiffness changes from k_{el} to k_s while

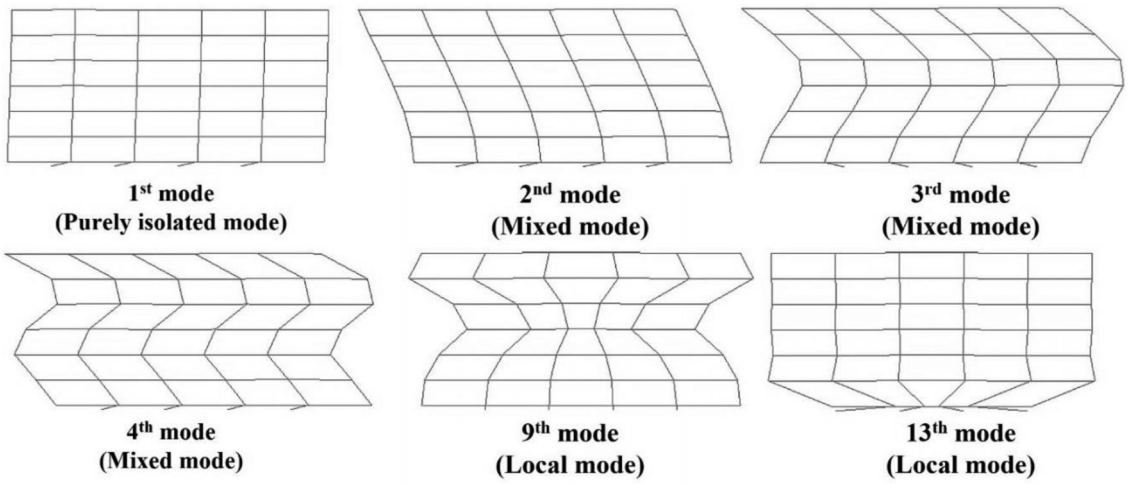

FIGURE 1 Example of mode shapes of a seismically isolated building in two-dimensional representation

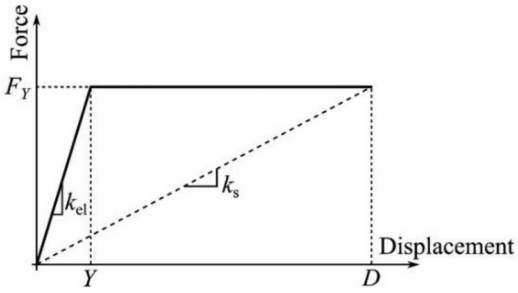

FIGURE 2 Elastoplastic behavior for demonstrating "damping leakage" or "spurious damping"

C and m are constant, the value of β changes from β_1 to β_2, where $\beta_2 = \beta_1 \bullet \sqrt{(k_{el}/k_s)} = \beta_1 \bullet \sqrt{(Y/D)}$. For $\beta_1 = 0.02$, $Y = 1$ mm and $D = 500$ mm (this is representative of response for the MCE_R), the effective damping becomes equal to 0.447 and significantly suppresses the isolation system displacements.[12] To eliminate such unintended damping, it has been proposed to use various forms of modal damping[12] for isolated buildings and the use of other forms of modal damping[16] or virtual viscous dampers with limits on the peak damping force ("capped viscous damping[15,17]") for the analysis of non-isolated buildings. For isolated buildings, it is recommended that the stiffness matrix used for the construction of the global damping matrix be formulated using the purely isolated modes (Figure 1) with the effective first modal period calculated using the post-elastic isolator stiffness (or a lesser value) and that constant modal damping be assigned to the remaining modes.[12] Early studies of Hall[18,19] used virtual viscous dampers for modeling damping in the superstructure of isolated buildings based on a different approach than the one used in this paper. They computed values of the damping constant for the virtual dampers utilizing the first mode of the isolated building after removing the isolator elements.[19] In this paper, the damping constants for the virtual dampers are computed using the second mode of isolated building without removing the isolator elements. We provide a discussion in Section 4.2 that this is a more appropriate approach for modeling damping in isolated buildings.

While implementation of the procedure of Sarlis and Constantinou[12] is easy in program SAP2000,[20] it is not possible to directly do so in many other programs, including OpenSees.[21] In an effort to alleviate this problem, Kitayama and Constantinou[22–24] added artificial springs below the isolation bearings that are only active during the initial stage of the analysis when the modal properties are computed, and the global damping matrix is constructed. While the authors have used this approach in their studies, they recognized that: (a) there are other proposals for modeling inherent damping for seismically isolated buildings and (b) other damping models proposed for non-isolated buildings have potential for use in seismically isolated buildings. Accordingly, this study evaluates the effect that different inherent damping models have on the results of a seismic performance assessment of selected seismically isolated buildings.

The following six models of inherent damping are considered: (a) Modal damping, (b) Zero damping, (c) Zareian-Medina damping, (d) Virtual dampers with force cap, (e) Virtual dampers without force cap and (f) Virtual dampers with the same damping constant at all stories without force cap. The zero damping or "undamped" model was used in seismic performance assessment studies of seismically isolated buildings by others.[25] These models were applied in an approach that satisfies the following conditions: (i) it eliminates or minimizes the problem of "damping leakage" in the isolation system, (ii) it is separated from and does not duplicate the action of hysteretic or frictional damping in either the structural elements or the seismic isolators, and (iii) the computational cost of inelastic time-history analysis is not substantially increased. Details of these damping models are provided in a special section in this paper. Moreover, the (somewhat popular) tangent stiffness proportional damping (i.e., through use of a stiffness matrix that is updated in every time step) was not utilized as it was observed that (i) there was a substantial increase in the computational time of inelastic time-history analysis, and (ii) there were frequent numerical convergence problems. The difficulties of using time-dependent properties for modeling inherent damping for seismically isolated buildings were previously reported by Pant.[11] Furthermore, Chopra and McKenna[16] recommended against the use of the tangent stiffness matrix to construct an instantaneous damping matrix because it lacks a physical basis and has conceptual implications including negative damping at large displacements.

While the analyses in this paper utilize the nonlinear direct-integration time-history method in program OpenSees[21] and concentrate on seismically isolated buildings with sliding isolation bearings (triple friction pendulum or TFP and double concave bearings or DC[26]), the findings are expected to be applicable to other isolation systems and other analysis programs.

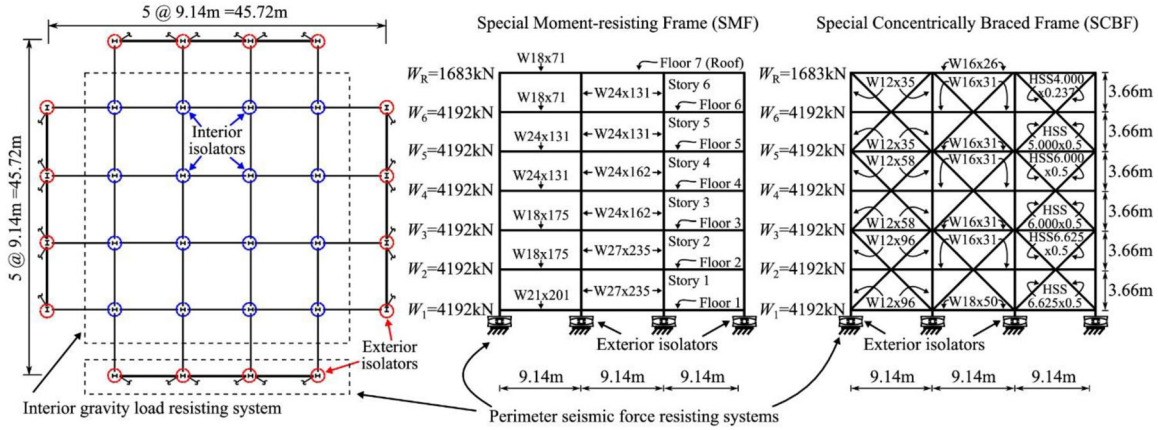

FIGURE 3 Plan and elevation of analyzed seismically isolated buildings

Past studies[10–12,14] also investigated the effect of superstructure damping on the response of seismically isolated buildings, in terms of peak floor acceleration, peak isolator displacement and peak story drift for specific seismic intensities (e.g., scaled for design level earthquake), using a small number of ground motions and assuming elastic behavior of the superstructure. The study of this paper investigates the effect of the superstructure damping modeling on the probabilistic response of isolated buildings designed by the procedures of the ASCE/SEI 7 standard,[27] considering ground motions of a wide range of seismic intensities (with return periods ranging from 43 to 10,000 years) and with due consideration for the inelastic response of the superstructure, and possible collapse of the superstructure and the isolation system. Results are obtained in terms of mean annual frequencies of exceedance for various parameters (peak floor acceleration, peak isolator displacement, peak story drift and peak residual story drift), and in terms of probabilities of collapse given the maximum considered earthquake (MCE_R)[27].

2 | DESCRIPTION OF ANALYZED BUILDINGS

The plan and elevation of the analyzed building are shown in Figure 3. The original design of this building was presented in SEAONC Volume 5 Seismic Design Manual[28] and McVitty and Constantinou.[29] The seismic weight at each floor was based on previous studies.[28,29] The building was assumed located on soil class D in San Francisco, CA (Latitude 37.783°, Longitude -122.392°) with Risk-Targeted MCE_R[27] spectral acceleration values of $S_{MS} = 1.5\,g$ and $S_{M1} = 0.9\,g$. The seismic force resisting frames for the superstructures were designed for $R_I = 2$ and detailed as Special Moment Resisting Frame (SMF) or as Special Concentrically Braced Frame (SCBF). Figure 3 presents the sections of columns, beams, and braces for the isolated buildings. Figure 3 also includes information of seismic floor weights.

The seismic isolation system considered in this study consisted either of TFP isolators with stiffening behavior and without a moat wall, or TFP isolators with a moat wall or DC isolators without a moat wall. The ultimate behavior of the TFP isolation system with a moat wall is effectively the same as that of a DC isolation system with a moat wall. These isolation systems were designed based on the minimum requirements of Section 17 of ASCE/SEI 7–16.[27] Identical bearings were placed at each of the columns of the building but because of the differences in gravity load, the isolators were modeled with different frictional properties at the inner and outer locations. McVitty and Constantinou[29] and Kitayama and Constantinou[22] presented details of the selection of the properties of the isolators based on prototype bearing tests and application of bounding analysis principles. Figure 4 presents the geometric and frictional properties of the isolators. The frictional properties are the lower bound values as those resulted in the largest displacements and probabilities of collapse. Figure 4 also presents force-displacement loops of the TFP and the DC isolators. Note that the moat wall is placed at displacement D_M and initiation of stiffening occurs at D_M, where D_M is the maximum isolator displacement as computed by the procedures of ASCE/SEI 7–16.[27] The DC isolators lack restrainer rings, which has been a common practice in Europe.[30] It is noted that the European Standard EN15129[31] (Section 8.3.1.2.3) prohibits the use of restrainer rings while ASCE/SEI 7–16[27] does not have such requirement. Also, the TFP isolators lack interior restrainer rings which nowadays is a common practice.[32] When the DC isolation system is equipped with a moat wall placed at the same location as that of the TFP system as shown in Figure 4, the two systems have effectively the same ultimate behavior. Accordingly, results related to the ultimate behavior, such as the probability

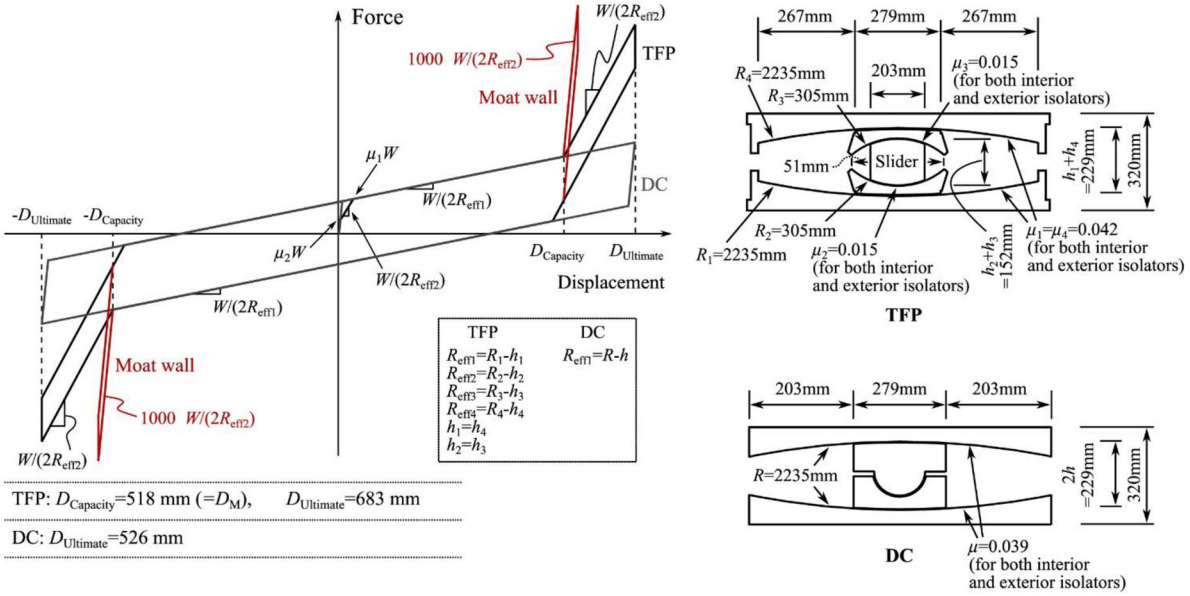

FIGURE 4 Drawings and force-displacement loops of triple FP and DC isolators

of collapse, obtained for the TFP system with a moat wall also apply for the corresponding DC system with a moat wall.

3 | MODEL FOR ANALYSIS

The analysis was performed in program OpenSees[21] using a two-dimensional representation of the structure as illustrated in Figure 5. The models used in this study are similar to those that were used in the previous studies by the authors[22–24,33,34] but slightly simplified for the purpose of the research discussed in Section 1 in this paper (particularly, the panel zone[35] was not explicitly modeled in this study). The models use the concentrated plasticity elements (nonlinear spring hinges) for the beams and columns and the distributed plasticity elements (fiber sections) for the braces.[36] The elastic stiffness of beam-column elements between the concentrated plasticity springs was selected based on Ibarra and Krawinkler[37] so that the equivalent stiffness of the "rotational spring—elastic beam-column element—rotational spring" assembly was equivalent to the stiffness of the actual frame members.

Figure 5 presents the model for the seismically isolated buildings with moment frame and braced frame. The frames were modeled in their principal direction. The seismic force resisting frames in the perpendicular direction were not considered. Seismic ground motion was considered only in the principal (horizontal) direction with only horizontal ground motion. In the models in Figure 5, each of the columns of the seismic force-resisting frame was supported by two isolator models. One of the isolator models represents two internal isolators and the other one represents two exterior isolators (i.e., contracted models). Note that interior and exterior isolators support different weights due to the locations of these isolators (see Figure 3). Only half of the building was modeled (i.e., the total seismic weight of the building is 53,670 kN, but the seismic weight of the modeled building was 26,835 kN). Tributary weights are also shown in the figure. Seismic masses to the horizontal direction were assigned at the beam-to-column intersections in the seismic force-resisting frames (i.e., at four nodes at each floor). The elements of the building other than the SMF or the SCBF (i.e., the gravity supporting frames) were also modeled using leaning columns with the beams assumed to be simply connected to the columns. Two sets of gravity load carrying leaning columns, one on the left and one on the right side of either the SMF or the SCBF are linked to the frame to simulate P-Delta effects. The leaning columns are modeled using elastic beam-column elements and low-stiffness rotational springs. These columns have moments of inertia and areas 100 times larger than the columns used for the first story in order to approximately represent the aggregate effects of all the gravity columns.[38] Truss elements are used to link the SMF or the SCBF to the leaning columns and transfer the P-Delta effect. The truss elements have areas 100 times larger than the frame columns in the first story to represent aggregate effect of all the gravity beams and are assumed to be axially rigid.[38]

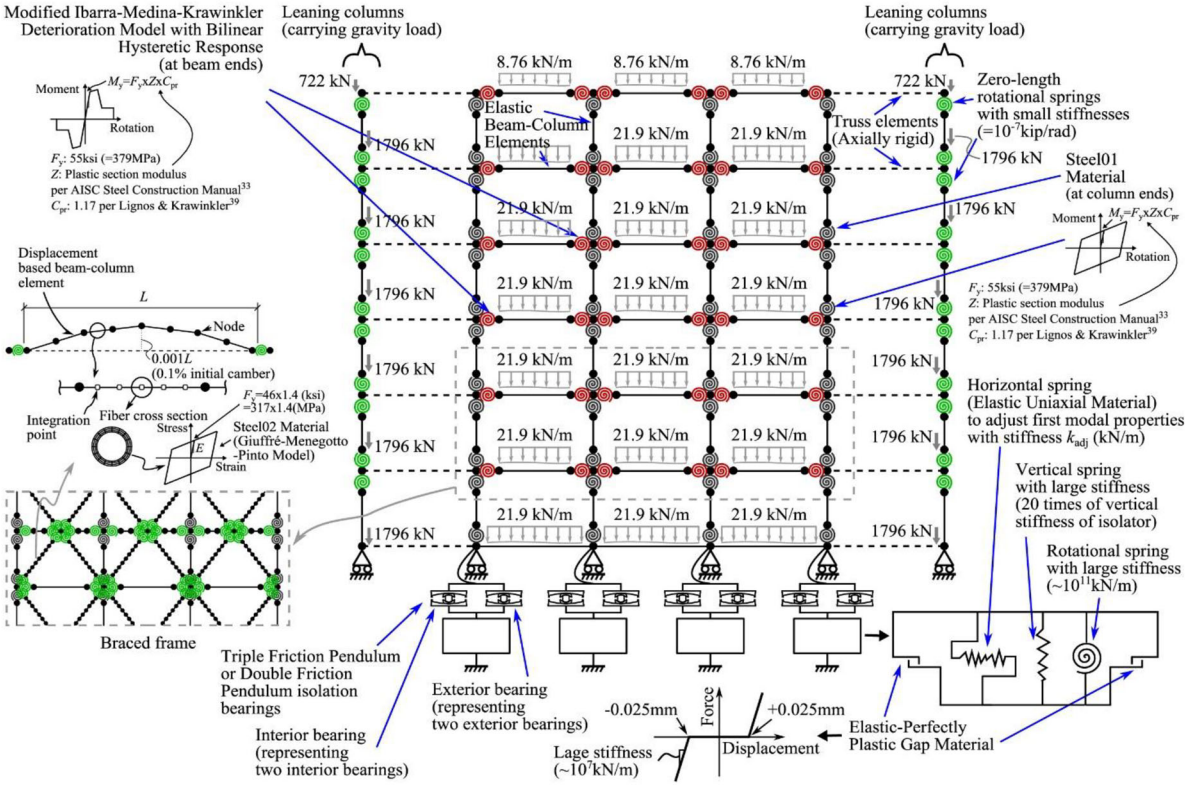

FIGURE 5 Model of six-story seismically isolated building (with artificial springs below isolators for constructing the global damping matrix)

The model (see Figure 5) features artificial springs below the isolators that are active only during the initial phase of the analysis so that the global damping matrix is properly constructed.[22–24] The springs feature a gap (modeled using the "Elastic-Perfectly Plastic Gap Material" in OpenSees, see Figure 5) of 0.025 mm. The gap did not cause any numerical problems.

For the model of SCBF, the braces consisted of eight displacement-based fiber elements that are capable of tracing flexural buckling (see Figure 5). In this study, braces were modeled to capture flexural buckling (fracture was not modeled as previous study by the authors[24] showed that it did not affect the results of seismic performance assessment of seismically isolated buildings). The flexural buckling was modeled based on the recommendations of Karamanci and Lignos[39] that was based originally on the study by Uriz and Mahin.[40] The parameters to model the braces are identical to those listed in Table 4 in Kitayama and Constantinou.[24] Note that the connections between braces and their gusset plates were not modeled but instead, the braces were directly pinned-connected to the beam to column intersections with zero-length rotational springs with a near-zero rotational stiffness. An initial camber of 0.1% of the total brace length was applied at the brace midpoint to initiate buckling.

For the model of SMF, the model was developed with due considerations for the ultimate behavior of the beams and columns based on Eads.[38] Important details of the model were: (a) rotational springs at the ends of beams were modeled using the Modified Ibarra-Krawinkler bilinear-hysteretic model,[41] which is capable of simulating deteriorating hysteretic moment-rotation relationship, and (b) rotational springs at the ends of columns were modeled using the bi-linear hysteretic element "Steel01 material" in OpenSees[21] without strength or stiffness deterioration and with a ratio of elastic to post-elastic stiffness equal to 0.002.

The TFP isolators were modeled using a modification of the series model.[42,43] The DC isolators were modeled using a bi-linear hysteretic model (based on the Steel01 material in OpenSees[21]). These models can simulate the behavior of the isolators depicted in Figure 4. When moat walls were considered, the same isolators models were used but the moat wall was placed at a distance equal to D_{Capacity} of the isolator, which was equal to displacement D_{M}. The isolation system (when moat wall was considered) behaved as shown in Figure 4 but with a much higher stiffness beyond displacement D_{Capacity}. Analyses with values of the stiffness equal to 1000 times the stiffness of the TFP isolator in the stiffening regime were used to model the moat wall. This moat wall model was also used in the previous studies by the authors.[22,23,33,34] It

should be noted that earlier studies[22] established that the value of the moat wall stiffness has an insignificant effect on the collapse performance. Specifically, results on the probability of collapse in the MCE_R were essentially the same when the stiffness varied from 50 to 1000 times of the value of the TFP isolation system stiffness in the stiffening regime. Also, the moat wall model features some hysteresis as seen in the loops of Figure 4, which results from the frictional behavior of the TFP. Other moat wall models exist.[19,44–46] The effect of using different models of moat wall on the seismic performance of seismically isolated buildings is out of the scope of this paper-it is conceivable that the use of different moat wall models may have some effect on the results presented in this article.

Finally, the TFP and DC isolator models feature linear elastic vertical stiffness which was calculated as half of the isolator column stiffness using the area of the slider as the column area.[12] That is, the vertical stiffness $k_{VC} = A_{Slider} \bullet E/(2H_{TFP})$, where A_{Slider} is area of slider (diameter of 203 or 279 mm), E is Young's modulus of steel (200,000 MPa) and H_{TFP} is height of the bearing (320 mm). This estimate of stiffness is considered an upper bound on the vertical stiffness.

4 | MODELING OF INHERENT DAMPING

4.1 | Modeling inherent damping using modal damping

The damping matrix, $\mathbf{C_{Modal}}$, is constructed as follows (known as the Wilson-Penzien damping)[16,47,48]:

$$\mathbf{C_{Modal}} = \mathbf{\Phi^T c \Phi} \tag{1}$$

$$\mathbf{c} = \mathbf{m}\left(\sum_{n=1}^{N} \frac{2\zeta_n \omega_n}{M_n} \boldsymbol{\phi_n} \boldsymbol{\phi_n^T}\right)\mathbf{m} \tag{2}$$

$$M_n = \boldsymbol{\phi_T^n} \mathbf{m} \boldsymbol{\phi_n} \tag{3}$$

where $\boldsymbol{\phi_n}$ is the n^{th} mode shape of the undamped system, $\mathbf{\Phi} = [\boldsymbol{\phi_1}, \boldsymbol{\phi_2}, \ldots, \boldsymbol{\phi_N}]$ is a matrix containing in its columns the mode shapes, $\mathbf{m}$ is a mass matrix, ζ_n is the n^{th} mode damping ratio, and ω_n is the n^{th} mode frequency. This approach allows for specification of the desired damping ratio in each mode of vibration.

For this study, the damping ratio was specified as 2% of critical in all modes except for the "purely isolated" modes (first mode in the two-dimensional models used) for which the damping ratio was set equal to zero per directions in Sarlis and Constantinou.[12] In the modal damping model, the elastic properties of the structure were used to construct the global damping matrix, which was then used in the nonlinear response history analysis. The application of the procedure for the isolated building model is complicated by the fact that the isolated building models are extremely stiff in the elastic range (for sliding systems, the elastic stiffness is the friction force at initiation of motion divided by some very small "yield" displacement, u_y, which in the model of this study was set equal to 1 mm). To appropriately construct the damping matrix, artificial horizontal, vertical, and rotational springs were placed below each isolator element to represent the desired stiffness for the construction of the damping matrix as depicted in Figure 5. These springs were restrained to only deflect by 0.025 mm in the horizontal direction so that in the nonlinear response history analysis they did not affect the behavior of the isolators. The horizontal stiffness of these artificial springs, k_{adj} (see Figure 5), was calculated by assuming that springs with the elastic stiffness k_{el} of isolators and the stiffness k_{adj} of the artificial springs are connected in series to result in post-elastic stiffness k_d of isolators so that (W is the total weight of the building model, 26,835 kN, $R_{effl} = R_1\text{-}h_1$; μ_2 is the coefficient of friction of surface 2; see Figure 4):

$$k_d = \frac{W}{2R_{eff1}} \tag{4}$$

$$k_{el} = \frac{\mu_2 W}{u_y} \tag{5}$$

$$k_{adj} = \frac{k_{el}\, k_d}{k_{el} - k_d} \tag{6}$$

For simplicity, the total value of stiffness k_{adj} was calculated (for all isolators) and then divided by the number of horizontal artificial springs with k_{adj} (= 4 in Figure 5) below isolators. Moreover, the frequency below which the damping ratio was set equal to zero ("purely isolated mode") was set equal to the inverse of the period based on the post-elastic stiffness, computed as $2\pi\sqrt{\frac{2R_{eff1}}{g}}$. This damping model will be called in the rest of this paper as "Modal" for brevity.

The artificial springs (soft springs) are necessary so that seismically isolated buildings have proper modal shapes to be able to properly construct the damping matrix. Without using the artificial springs, the modes of a seismically isolated building are computed in program OpenSees using the initial stiffness of isolators, which is very large. The first mode vibration should be the "purely isolated mode" (as shown Figure 1), which can be obtained only when using small stiffness for the isolation system. Also, we observed that when "modal damping" was used in the SCBF with DC isolators without a moat wall, the "damping leakage" problem could occasionally occur. This was avoided by using a slightly larger gap than 0.025 mm (Figure 5) (e.g., 0.05 mm) or using a smaller value for the stiffness for the artificial springs (smaller than $W/2R_{eff1}$, as also recommended by Sarlis and Constantinou[12]).

4.2 | Modeling inherent damping using virtual linear viscous dampers

A recent study by Qian, Chopra and McKenna[49] made use of virtual linear viscous dampers to model inherent damping. The damping constant C_j (j denotes story number—see Figure 3) for the viscous dampers is considered proportional to the story stiffness K_j, that is, $C_j = \alpha K_j$ (α is a factor to be determined; one damper is used for each story in the model used for nonlinear response history analysis). The relationship between the damper force at story j, $F_{d,j}$, and the relative velocity $\dot{u}_j$ between the adjacent floors is written as:

$$F_{d,j} = C_j \dot{u}_j = \left(\alpha K_j\right) \cdot \dot{u}_j \tag{7}$$

The study by Qian, Chopra and McKenna[49] imposed limits on the positive and negative damping forces ("caps"). The use of force caps was originally proposed by Hall.[15] In these studies,[15,49] the damping forces are capped at $2\zeta_m$ times the yield strength (or peak shear strength) of each story, where ζ_m is the damping ratio for m^{th} mode vibration. For non-isolated structures, the $m = 1$ was used.[15,49] The story stiffness K_j in Equation (7) may be computed as the elastic stiffness which is computed from the value of $2\zeta_m$ times the yield strength and the corresponding story drift from the push-over analysis or linear response history analysis. The modal damping ratio ζ_m for the six-story analyzed seismically isolated buildings is given by the following equation:

$$\zeta_m = \frac{T_m}{4\pi} \cdot \frac{\sum_{j=1}^{6} C_j \cdot \cos^2\theta_j \cdot \delta_{j,m}^2}{\sum_{i=2}^{7} w_i/g \cdot \varphi_{i,m}^2} = \frac{T_m}{4\pi} \cdot \frac{\sum_{j=1}^{6} \left(\alpha \cdot K_j\right) \cdot \cos^2\theta_j \cdot \delta_{j,m}^2}{\sum_{i=2}^{7} w_i/g \cdot \varphi_{i,m}^2} \tag{8}$$

where T_m is the m^{th} modal period, w_i is the seismic weight at the i^{th} floor (it starts from $i = 2$ as the first floor mass, $i = 1$, is related to the level where isolation devices are located [below 1st floor] and the inherent damping is not considered at that level), $\varphi_{i,m}$ is the m^{th} modal displacement at i^{th} floor, θ_j is the angle of inclination of damper at j^{th} story, and $\delta_{j,m}$ is modal drift for j^{th} story (= $\varphi_{i,m}$-$\varphi_{i-1,m}$) for m^{th} mode. Note that the modal displacements used were normalized so that the top floor modal displacement is equal to unity. Note that the Equation (8) is based on Qian, Chopra and McKenna[49] but adjusted by adding the cosine-terms for the effect of the angle of inclination of the dampers based on Ramirez.[50] A recent study by Anajafi[14] made use of a simplification of Equation (8) and used the second mode of vibration (or mixed mode as shown in Figure 1) but did not include damper force caps. The use of the second mode of vibration is important as it is associated with deformation of the superstructure as seen in Figure 1.

In this study, the inherent damping is modeled using virtual linear viscous dampers based on the approach described above with use of Equation (8) and based on the modal properties of second mode of vibration ($m = 2$). The stiffness K_j was obtained from static pushover analysis using a lateral force distribution proportional to the floor mass (= w_i/g) times the second modal displacements (= $\varphi_{i,2}$). Unlike the study of Anajafi[14] which modeled the building superstructure using linear elastic elements and did not include the force-cap for the dampers (based on the observation that the peak damper forces in limited number of nonlinear response history analyses were small—about 0.01 W,

where W is the total seismic weight), the building of this study (see Figure 5) was modeled using nonlinear elements to simulate yielding of beams, columns, and braces, and the design base shear forces (per seismic force resisting frame) that was used to design the buildings with $R_I = 2$ were 3930 kN/2 = 1965 kN and the seismic weight (half of the building; see Figure 1) was 26845 kN. Thus, the $F_y/W \approx 1965$ kN/26835 kN ≈ 0.07. By comparison, in the Anajafi,[14] the damper peak force was 0.01 W, which as portion of the yield force is $0.01W \approx 0.01 \bullet (F_y/0.07) = 0.14F_y$, which exceeds the force corresponding to the recommended cap limit of damper force per Hall[15] and Qian, Chopra and McKenna.[49] This limit is $2\zeta_m F_y = 2 \bullet 0.02 \bullet F_y = 0.04F_y$ (when 2% inherent damping is used). Thus, the cap limit in the damper force needed to be included in the damping model. Hereafter, this damping model is called "Dampers,wCap" for brevity.

Additionally, other simpler models are considered in this study, as the authors noticed that the inclusion of force-cap in dampers slowed down the speed of computation of nonlinear response history analysis in OpenSees (possibly due to the abrupt change in damping force at the force cap). Also, the computation of story stiffness requires additional analysis (push-over analysis or linear response history analysis as recommended per Qian, Chopra and McKenna[49]) that are dependent on the types of lateral force distribution (in the case of pushover analysis) and on the selection of ground motion records used for linear response history analysis. Thus, the following two additional simpler models were considered:

- Same as above but with the force cap removed,
- Same as above but with the force cap removed and the damping constants C_j made to be the same for all stories (identical virtual dampers at each story).

Hereafter, these additional damping models are called "Dampers,w/oCap" and "Dampers,SameC", respectively, for brevity.

Note that artificial springs as described in Section 4.1 and depicted in Figure 5 to control the modal characteristics of buildings are still needed in the computation of stiffnesses and modal periods and displacements for use in Equation (8) to compute C_j. However, they are not needed for the nonlinear response history analysis when "Dampers,wCap" or "Dampers,w/oCap" or "Dampers,SameC" is used to model inherent damping.

Figure 6 presents the results of pushover analysis for seismically isolated buildings with SMF (top row) and SCBF (bottom row). The figures on the left show the story shear force versus the story drift ratio for each story when the lateral forces in the pushover analysis are based on the second mode vibration ($m = 2$) of the seismically isolated building. The peak story shear force or strength was used to compute the cap force for each damper (i.e., using $2\zeta_m F_{y,j}$, where $F_{y,j}$ is the peak strength of each story j). Also, the stiffness K_j to implement Equation (7) were obtained based on $2\zeta_m F_{y,j}$ and the corresponding displacement from the pushover curves.

It is seen from the Figure 6 (left) that the first and second stories did not yield. Therefore, the force cap of the dampers at the first and second stories were determined based on the results of pushover analysis using first mode lateral forces. The center graphs in Figure 6 show the pushover curves in this case. Also, the right graphs of Figure 6 show base shear force vs roof drift ratio for the two cases of loads based on the first and second modes. It is seen in the graphs on the right that the isolation bearings did not move (slide) in the pushover analysis for lateral loads that were proportional to the second mode displacements. This demonstrates that the second mode of vibration in seismically isolated buildings is dominated by superstructure deformation.

In modeling the dampers with and without force caps in OpenSees,[21] the twoNodeLink element with BilinearOilDamper material was used. The BilinearOilDamper material[51] was used to model dampers as this uniaxial material allows users to specify "caps" in the damper force. Figure 7 illustrates how the dampers were placed in the model in OpenSees.

4.3 | Modeling inherent damping using element-specific initial stiffness proportional damping

Zareian and Medina[52] proposed, for non-isolated buildings, a model of inherent damping in which the global damping matrix is constructed using the stiffness proportional method (a subset of the Rayleigh method[48]) with a constant stiffness matrix that is assembled by assigning zero stiffness-proportional damping to structural elements that may experience inelastic deformations. The moment frames in Zareian and Medina[52] were modeled using concentrated plasticity elements (nonlinear spring hinges) for the beams and columns, and with linear elastic representation of the

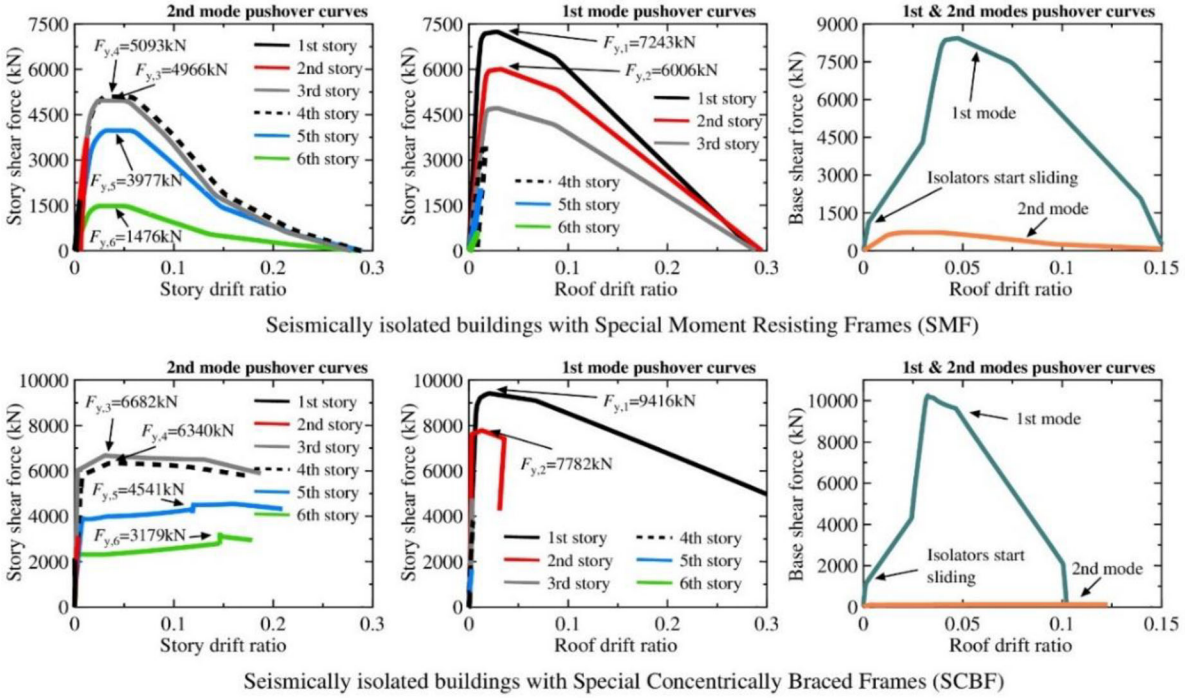

FIGURE 6 Pushover curves of seismically isolated building. Left: Story shear force vs story drift ratio-loads proportional to second mode. Center: Story shear force vs story drift ratio-loads proportional to first mode. Right: Comparison of base shear vs roof drift ratio curves based on first and second modes

beam-column elements between the concentrated plasticity springs[37] as done in this study and described in Section 3. In the stiffness proportional damping method, the damping ratio ζ is proportional to ω, is expressed by the following equation[48]:

$$\zeta = \frac{a_1.\omega}{2} = \frac{2.\zeta_m}{\omega_m}.\frac{\omega}{2} \tag{9}$$

where a_1 is the coefficient by which the stiffness matrix is multiplied to obtain the damping matrix ($= 2\zeta_m/\omega_m$, ω_m is the frequency of m^{th} mode, ζ_m is the damping ratio of the m^{th} mode). In this study, the coefficient a_1 was computed using the second mode frequency. For the buildings with SMF, $\zeta_2 = 0.02$ and $\omega_2 = 6.78$ rad/sec, and damping was assigned to the beams and columns that were modeled by elastic-beam column elements (damping was not assigned to any yielding springs). For the buildings with SCBF, $\zeta_2 = 0.02$, $\omega_2 = 16.73$ rad/sec, and damping was assigned to the beams and columns that were modeled by elastic-beam column elements, and to the braces that were modeled by displacement-based beam-column elements with fiber cross sections that can simulate nonlinear elasto-plastic behavior. Note in modeling inherent damping for seismically isolated buildings, use of artificial springs below the isolators (see Figure 5) is still needed to properly form the stiffness matrix and avoid "damping leakage" problems. Hereafter, this damping model is called "Zareian-Medina" for brevity.

Figure 8 shows the dependency of the damping ratio, ζ, on frequency for the considered damping models of Sections 4.1, 4.2, and 4.3. Equations (1) to (3) were used to compute damping ratio for the "Modal" case, Equation (8) was used for the cases of "Dampers, wCap," "Dampers, w/oCap," and "Dampers, SameC" and Equation (9) was used for the "Zareian-Medina" case. It is seen that all damping models have 2% (= 0.02) damping ratio at the second modal frequencies (the dots in the figure denote the modes). Also, in the case of SMF, the Zareian-Medina model diverges from other models and results in higher values of the damping ratio for modes higher than the 3$^{\text{rd}}$, whereas in case of the SCBF, the same model diverges from other models after 7$^{\text{th}}$. These relationships are used in the next section of this paper to provide interpretation of the results of seismic performance assessment of seismically isolated buildings when the superstructure remains elastic.

Note that in the braced frame buildings of this study, the "modal damping" and "Zareian-Medina" damping methods were used in structures with braces which were modeled using distributed plasticity models. Chopra and McKenna[16]

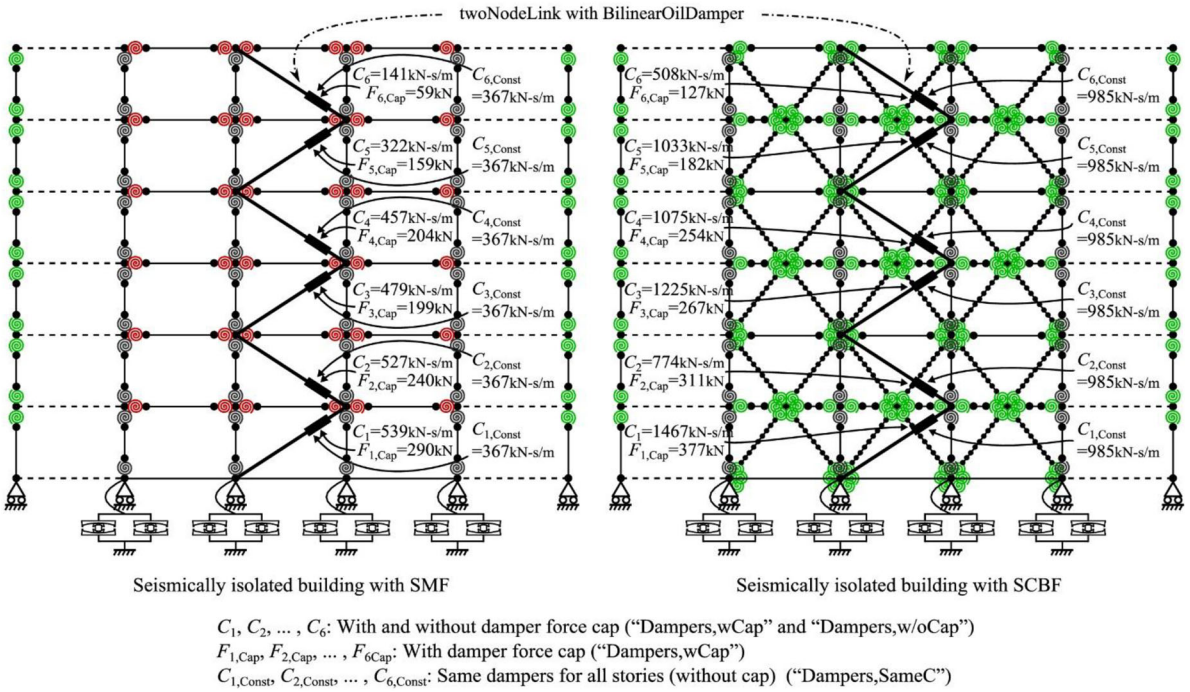

FIGURE 7 Inherent damping models with virtual viscous dampers

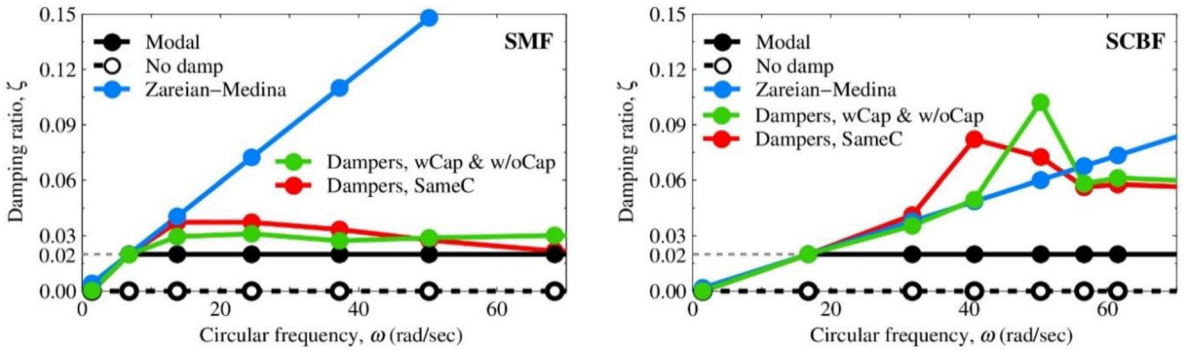

FIGURE 8 Damping ratio as function of frequency (and mode) for various damping models for the analyzed seismically isolated buildings

compared the seismic response of 20-story non-isolated buildings modelled by distributed plasticity elements (like the braces in this study). They observed that a damping amplification problem did not occur when distributed plasticity elements were used. Accordingly, we used the "modal damping" and "Zareian-Medina" methods and applied damping to the braces, which were modeled using distributed plasticity elements.

5 | EFFECT OF INHERENT DAMPING MODEL ON SEISMIC PERFORMANCE

For the seismic performance evaluation of this study, the mean annual frequency of exceeding the engineering demand parameters (EDPs) of peak floor acceleration, peak story drift ratio, peak residual story drift ratio, and peak isolator horizontal displacement are considered. These EDPs are indicators of damage to the structural and non-structural systems and the contents of the buildings.[53] The peak isolator horizontal displacement is important in assessing failure of the seismic isolation system and collapse of the building. Also, collapse fragility curves for the buildings are constructed and used to assess the effect of the different inherent damping models on the collapse performance.

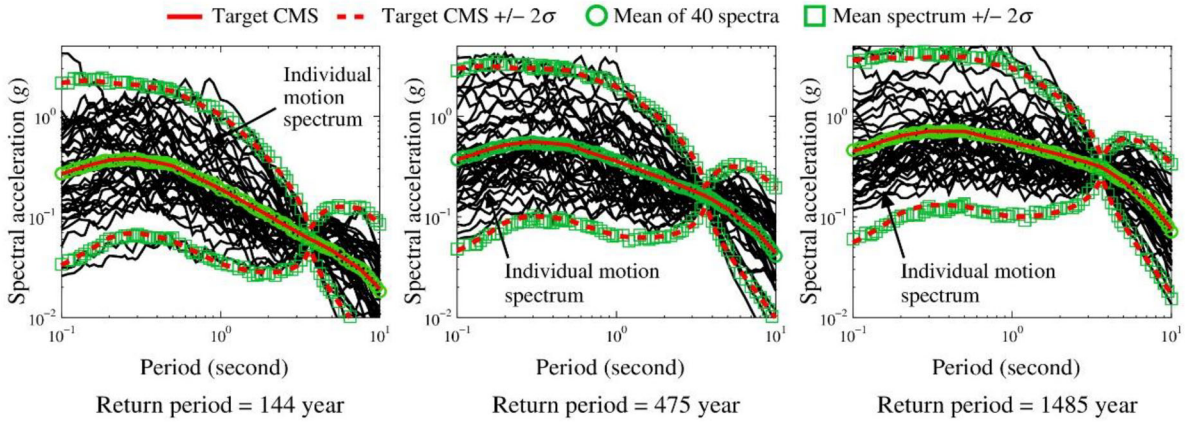

FIGURE 9 Acceleration response spectra (5%-damped) of motions used for response history analysis of seismically isolated buildings for return period of 144, 475, and 1485 years

5.1 | Selection and scaling of ground motions for nonlinear response history analysis

The records of ground motions used for nonlinear response history analysis are identical to those used in Kitayama and Constantinou.[22,24,33] Background information can be found in NIST[3] and Lin.[54] A total of 400 ground motions were selected and scaled to represent ten different seismic intensities (40 records for each intensity) as measured by the earthquake return periods of 43, 144, 289, 475, 949, 1485, 2475, 3899, 7462 and 10,000 years for period of 3.66 s that corresponds to the effective period T_M at the maximum isolator displacement, D_M (Section 17.5.3.2 in ASCE/SEI 7–16[27]). The multiple stripe analysis technique[55] was used for the analyses as it allowed for the use of different sets of hazard-consistent ground motions at each intensity level (i.e., return period). The results of the study are presented in the form of relationships between specific EDP values and the annual frequency of exceeding these EDP values. More information regarding the ground motion selection and scaling for the structures studied in this paper can be found in Kitayama and Constantinou.[22] As an example, selected and scaled ground motions for the seismic response analysis of seismically isolated buildings, target Conditional Spectra[3,54] with target variations of $\pm 2\sigma$, and Conditional Mean Spectra (CMS[56]) for three different return periods (144, 475, and 1485 years) are shown in Figure 9.

Details for each of the 400 ground motions used in the analysis, including peak values of acceleration, velocity and displacement, and time histories of acceleration, velocity, and displacement, are provided in a digital appendix.[57]

5.2 | Effect of inherent damping model on seismic performance of seismically isolated buildings

The mean annual frequency of a EDP exceeding a value y, $\lambda(\text{EDP} > y)$ was computed. The calculation of $\lambda(\text{EDP} > y)$ was based on NIST[3] and Lin[54] as follows:

$$\lambda\ (\text{EDP} > y) = \sum_{i=1}^{n} P\left(EDP > y | Sa\left(T_M\right) = x_i\right) \cdot \lambda\left(Sa\left(T_M\right) = x_i\right) \tag{10}$$

$$\lambda\ \left(Sa\ \left(T_M\right) = x_i\ \right) = 0.5\{\lambda\left(Sa\left(T_M\right) > x_{i-1}\right) - \lambda\left(Sa\left(T_M\right) > x_{i+1}\right)\} \tag{11}$$

where n is the number of considered spectral acceleration $Sa(T_M)$ amplitudes (in this study $n = 10$, the number of seismic intensities or return periods considered). x_i is the spectral acceleration at the period $T = 3.66$ s for i^{th} return period (see Figure 9). Also, $\lambda(Sa(T_M) = x_i)$ is the rate of observing $Sa(T_M)$ in some small range represented by the discrete amplitude x_i. $P(EDP > y|Sa(T_M) = x_i)$ is the probability of the EDP that exceeds a value of y conditioned at the intensity of $Sa(T_M) = x_i$. The calculation of $P(EDP > y|Sa(T_M) = x_i)$ depends on the EDP as follows[3,54]:

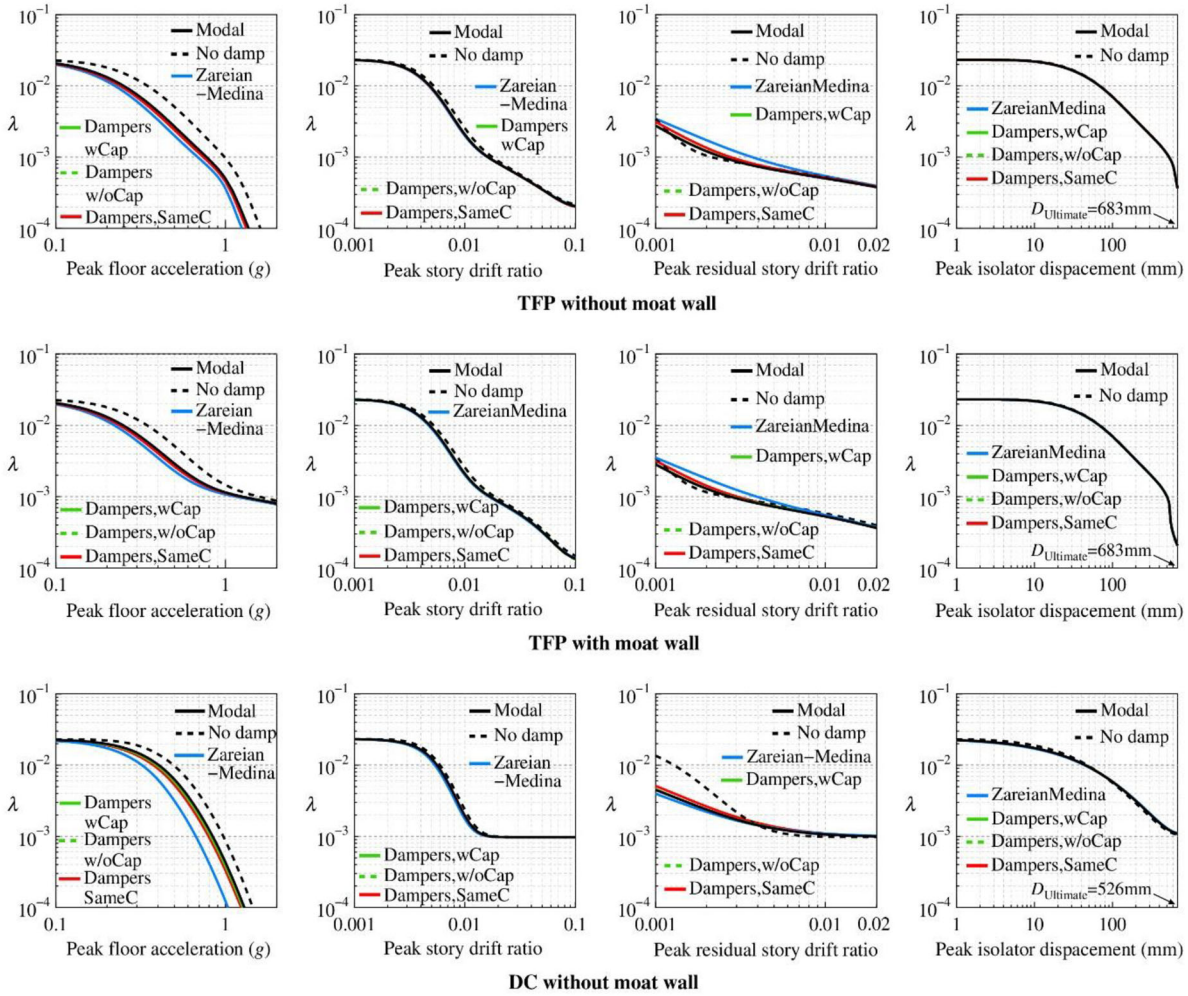

FIGURE 10 Mean annual frequencies of exceedance for various EDP of seismically isolated buildings with SMF

1. For the peak story drift ratio (EDP = *PSDR*):

$$P\ (PSDR > y|\, Sa\ (T_{\mathrm{M}}) = x_i\ ) = \ P\,(C) + (1 - P\,(C))\left(1 - \Phi\left(\frac{lny - \mu_{lnPSDR}}{\sigma_{lnPSDR}}\right)\right) \tag{12}$$

In Equation (12), μ_{lnPSDR} and σ_{lnPSDR} are the mean and standard deviation of *lnPSDR* values given $Sa(T_1) = x_i$ in which collapse did not occur. Note that $P\ (PSDR > y|Sa\ (T_{\mathrm{M}}) = x_i\ ) = \ 1$ was assumed when all 40 ground motions at a specific return period causes collapse of building. Φ is the normal cumulative distribution function. When collapse was observed in a nonlinear response history analysis, the peak story drift ratio was removed from the calculation of term "$\Phi(lny\text{-}\mu_{lnRSDR}/\sigma_{lnPSDR})$" in Equation (12). $P(C)$ is the probability of exceeding collapse limits given $Sa(T_{\mathrm{M}}) = x_i$. It was obtained by constructing a collapse fragility curve (i.e., cumulative distribution function) using the method of maximum likelihood.[58,59] Collapse was defined using the following criteria:

a. Collapse of the isolators when the lateral displacement exceeds D_{Ultimate} (see Figure 4).
b. Collapse of the superstructure when the story drift exceeds 0.05 for the SCBF[22,60] and 0.1 for the SMF.[22,61]
c. Instability as detected by termination of the analysis program due to large increment in story drift and/or large increment in isolator displacement over a small time strep.

2. For the peak residual drift ratio (EDP = *PRDR*) and the peak isolator displacement (EDP = *PID*), the same procedure applies with Equation (12) used but *PSDR* replaced by *PRDR* or *PID*. Note that $P\ (PRDR > y|Sa\ (T_{\mathrm{M}}) = x_i\ ) = \ 1$ and

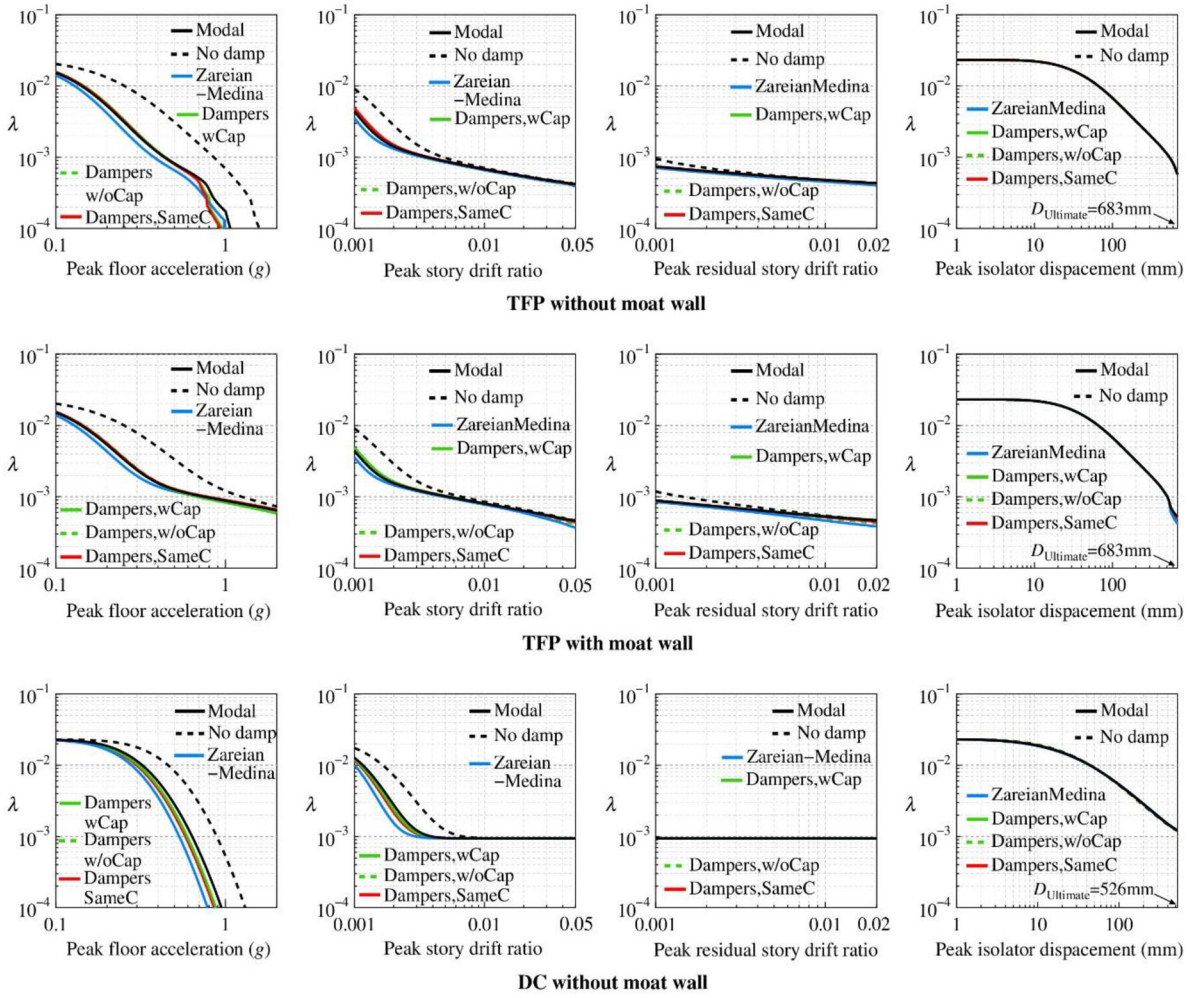

FIGURE 11 Mean annual frequencies of exceedance for various EDP of seismically isolated buildings with SCBF

$P\,(PID > y|Sa\,(T_{\mathrm{M}}) = x_i\,) = 1$ were assumed when all 40 ground motions at a specific return period causes collapse of building.

3. For the peak floor acceleration (EDP = *PFA*):

$$P\,(PFA > y|\,Sa\,(T_{\mathrm{M}}) = x_i\,) = 1 - \Phi\left(\frac{lny - \mu_{lnPFA}}{\sigma_{lnPFA}}\right) \tag{13}$$

Here, μ_{lnPFA} and σ_{lnPFA} are the mean and standard deviation of the *lnPFA* values given $Sa(T_{\mathrm{M}}) = x_i$. Note that $P\,(PFA > y|Sa\,(T_{\mathrm{M}}) = x_i\,) = 0$ was assumed when all 40 ground motions at a specific return period cause collapse of building. When collapse was observed in a nonlinear response history analysis, the peak floor acceleration was removed from the calculation of term "$\Phi(lny\text{-}\mu_{lnPFA}/\sigma_{lnPFA})$" in Equation (13).

Figures 10 and 11 present the computed $\lambda(\mathrm{EDP} > y)$ for the seismically isolated buildings with moment frames (SMF) and buildings with braced frames (SCBF), respectively. Evidently, there are major effects of the inherent damping modeling on the calculated mean annual frequencies of exceeding limits of the peak floor acceleration for both SMF and SCBF, especially when the inherent damping was zero ("No damp" in Figures 10 and 11). The inclusion of the inherent damping using the "Zareian-Medina" model consistently resulted in a noticeable reduction in the mean annual frequency of peak floor acceleration, due apparently to high damping in higher modes of vibration (see Figure 8). The underestimation of peak floor acceleration may have an impact on the seismic performance assessment of buildings when performance of acceleration-sensitive nonstructural components is considered. It is seen that the EDPs from other inherent damping models (i.e., "Modal," "Dampers, wCap," "Dampers, w/oCap," "Dampers, SameC") for both SMF and SCBF do not

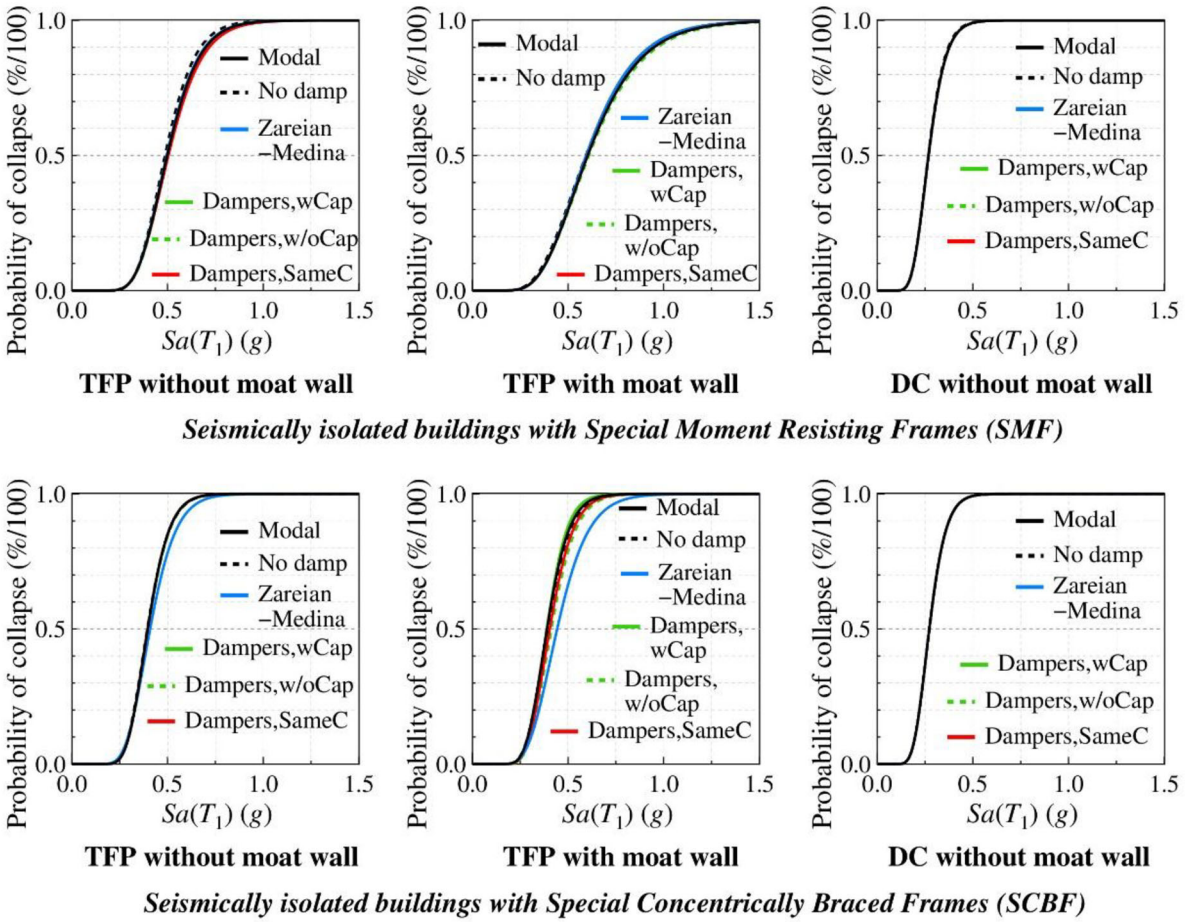

FIGURE 12 Collapse fragility curves of seismically isolated buildings for different inherent damping models

have noticeable differences. It is noted that regardless of which inherent damping models was used, the mean annual frequencies of peak isolator displacements were almost identical.

The results in Figures 10 and 11 apply for the case of superstructure inherent damping ratio of 0.02 in the first mode as seen in Figure 8 (also for zero damping). The value of 0.02 for the inherent damping is typically used for steel buildings.[62] However, the results and observations made above could have been affected by the small value of damping. Accordingly, the analysis was repeated having changed the value of damping to 0.05. Results are presented digital appendix,[57] where we observed the same trends as those seen in Figures 10 and 11 for the case of 0.02 damping ratio.

5.3 | Effect of inherent damping model on seismic collapse probabilities of seismically isolated buildings

Collapse fragility curves were constructed by fitting the empirical collapse data with a lognormal distribution. The empirical collapse data were in the form of the probability of collapse (number of collapse cases divided by the number of analyses) versus 10 distinct values of the seismic intensity as measured by the spectral acceleration at T_M (for return periods of 43–10,000 years). Figure 12 presents the collapse fragility curves of the isolated buildings for the five different inherent damping models. Each of the fragility curves is characterized by the median, $\widehat{Sa}_{\text{Collapse}}(T_M)$ (value of spectral acceleration for which the probability of collapse is 0.5), and the dispersion, β_{RTR}, which reflects the uncertainty of collapse capacity due to the record-to-record variability of the ground motions used in the nonlinear response history analysis. The results of Figure 12 show that the different inherent damping models have no effect on the collapse fragility curves for the isolated buildings except in the case of SCBF with the TFP system (with moat wall) and only when the "Zareian-Medina" damping model was used. In this case, the "Zareian-Medina" model underpredicted the probability of collapse.

TABLE 1 Collapse probabilities of seismically isolated buildings in MCE_R ($P_{Collapse,MCE}$)

	SMF			SCBF		
	TFP without moat wall	TFP with wall/DC with moat wall	DC without moat wall	TFP without moat wall	TFP with wall/DC with moat wall	DC without moat wall
Modal	3.9	2.7	41.5	10.2	11.3	39.8
No damp	4.1	3.0	41.9	10.6	11.3	39.8
Zareian-Medina	4.0	2.7	41.5	10.0	7.9	39.8
Dampers, wCap	3.9	2.6	41.5	10.2	10.7	39.8
Dampers, w/oCap	3.7	2.7	41.5	10.0	8.9	39.8
Dampers, SameC	3.9	2.7	41.5	10.2	9.8	39.8

Collapse fragility curves when the inherent damping is 0.05 rather than 0.02 are provided in the digital appendix,[57] where the same observations can be made as those related to Figure 12 for the case of 0.02.

5.4 | Effect of inherent damping model on the probability of collapse at MCE_R

While the fragility curves in Figure 12 show small differences when different inherent damping models are used, it is useful to compute the probabilities of collapse given the occurrence of the MCE_R. The probability of collapse at MCE_R is used to assess "acceptable" collapse performance of buildings in accordance with the Table 1.3-2 in ASCE/SEI 7–16 standard.[27] These probabilities may be affected when using different inherent damping models. The calculation of the probabilities of collapse given the occurrence of the MCE_R, $P_{Collapse,MCE}$, was computed as follows:

$$P_{Collapse,MCE} = \int_0^1 \frac{1}{s\beta_{TOT}\sqrt{2\pi}} \exp\left[-\frac{(\ln s - ACMR)^2}{2\beta_{TOT}^2}\right] ds \tag{14}$$

$$ACMR = \frac{\widehat{Sa}_{Collapse}(T_M)}{Sa_{MCE}(T_M)} \tag{15}$$

$$\beta_{TOT} = \sqrt{\beta_{RTR}^2 + \beta_{DR}^2 + \beta_{TD}^2 + \beta_{MDL}^2} \tag{16}$$

where $\widehat{Sa}_{Collapse}(T_M)$ is obtained from Figure 11 (explained in Section 5.3 in this paper), $Sa_{MCE}(T_M)$ is the spectral acceleration of MCE_R at T_M ($Sa_{MCE}(T_M) = 0.246\,g$), β_{TOT} is the total uncertainty, β_{DR} is the design requirements-related collapse uncertainty, β_{TD} is the test data-related collapse uncertainty and β_{MDL} is the modeling-related collapse uncertainty. The following quality ratings and related uncertainties were used: good with $\beta_{MDL} = 0.2$ for modeling; good with $\beta_{TD} = 0.2$ for test data and superior with $\beta_{DR} = 0.1$ for design requirements (same assumptions made in FEMA,[44] and Masroor and Mosqueda[63]).

Table 1 presents the computed value of $P_{Collapse,MCE}$ for each of the inherent damping models considered. In general, the different inherent damping models have insignificant or minor effect on the probability of collapse in the MCE_R. When a moat wall was used for seismically isolated buildings with SCBF and when the "Zareian-Medina," or "Dampers, w/oCap" or "Dampers, SameC" models were used (particularly the case of "Zareian-Medina"), the probabilities of collapse decreased slightly. This may be explained by the higher damping provided by these models as seen in Figure 8. While the difference in collapse probabilities between the high value (11.3%) and the low value (7.9%) for the SCBF with TFP/DC and a moat wall may not be significant, care may be needed when the moat walls are modeled and when stiff seismic force-resisting systems are used for the superstructure (such as braced frames or shear walls). It is also noted that there is almost no effect of the inherent damping model (including the case of zero damping) in the value of $P_{Collapse,MCE}$ when DC isolators without a moat wall were used. This implies that collapse was due to isolator failure rather than superstructure failure. Details on the number of collapses of each type considered (excessive drift, excessive isolator displacement or

numerical instability) for each of the analyzed systems, in each of the 10 seismic hazard intensities are presented in the digital appendix.[57] It should be noted that by counting the number of failures by type (excessive drift, excessive isolator displacement or termination of analysis) one may realize that there are combined types of failure in which there could have been excessive drift and excessive isolator displacement, or excessive drift and termination of the analysis. The digital appendix[57] includes also the computed probabilities of collapse in the MCE_R when the damping is 0.05 rather than 0.02, and again the same trends are observed as in the case of 0.02 damping. It may be noted that there is a small decrease in the probabilities of collapse for 0.05 damping when moat walls are used, likely due to reduction in the superstructure deformation caused by the higher inherent damping.

Note that this paper considered buildings designed using the minimum criteria for seismic isolation systems according to ASCE/SEI 7–16.[27] This led to unacceptably large probabilities of collapse for some seismic isolation system designs as seen in the results of Table 1. As shown in Figure 4, the force-displacement loops of TFP and DC are almost identical up to the initiation of hardening of TFP. If a moat wall is used in the DC isolation system at a displacement identical to that of the TFP, as shown in Figure 4, the two systems would have identical ultimate behavior that is controlled by the moat wall. Accordingly, the results of Table 1 on the probability of collapse for the TFP with a moat wall also apply for the nearly identical DC system with a moat wall.

5.5 | Effect of inherent damping model on seismic floor acceleration spectra

While the peak floor acceleration discussed in the Section 5.2 in this paper is used in the contemporary seismic performance assessment procedure in FEMA P58,[53] some non-structural components may be sensitive to spectral accelerations at other values of period.[64–68]

In this section, floor acceleration spectra are presented for each inherent damping model, for each seismically isolated building and for ground motions for the return period of 475 years. According to Molina Hutt,[69] the selected intensity level (= return period of 475 years) is representative of the expected earthquake defined by the San Francisco Planning and Urban Research Association to define resilience. This expected earthquake corresponds to a magnitude of 7.2 earthquake scenario, which is an event that can be expected conservatively, but reasonably within the lifetime of a structure. Figures 13 and 14 present the mean floor acceleration spectra for the seismically isolated buildings with SMF and SCBF, respectively, for the 1st, 4th and 7th floors. It is evident that when the inherent damping is zero (case "No Damp"), the floor acceleration spectra are much higher than the cases that inherent damping was properly modeled. The difference is significant for periods less than one second, where most secondary systems have their period. It is also observed that the floor acceleration spectra are consistently lower when the inherent damping model of "Zareian-Medina" was used, especially for periods less than one second, due to the higher damping this model provides in the higher modes of vibration. The results presented in Figures 13 and 14 demonstrate the significance of the inherent damping model in seismic performance evaluation of non-structural components. The insensitivity of inherent damping models in predicting floor spectral accelerations for periods larger than 1 s is because seismic isolation reduces deformations in the superstructure.

Results comparable to those of Figures 13 and 14 but for inherent damping of 0.05 rather than 0.02 are presented in the digital appendix.[57] The observations made for the case of 0.02 damping also apply for the higher value of damping.

6 | SUMMARY AND CONCLUSIONS

This study examined the effect of different inherent damping models on the seismic performance of seismically isolated buildings with steel special moment-resisting frames and steel SCBFs, which were designed using the minimum requirements of ASCE/SEI 7–16.[27] Three different isolation systems were considered: TFP isolators without moat walls, TFP isolators with moat wall and DC isolators without moat walls. The main difference between the TFP and the DC isolators was in the stiffening behavior of the TFP isolators which reduced the potential for collapse of the isolators (or eliminated collapse of the isolators when moat walls were used). DC isolators with moat walls have effectively the same ultimate behavior as TFP isolator with moat walls when the moat walls are placed as considered in this study. Accordingly, the collapse performance of the TFP system with moat walls is considered to also apply for the DC with moat walls. The inherent damping models examined were: (i) modal damping (called "Modal" in this paper), (ii) linear viscous dampers (called "Dampers,wCap," or "Dampers,w/oCap" or "Dampers,SameC" depending on the inclusion of limits in the damping force or specification of damping constants); (iii) element specific initial stiffness proportional damping

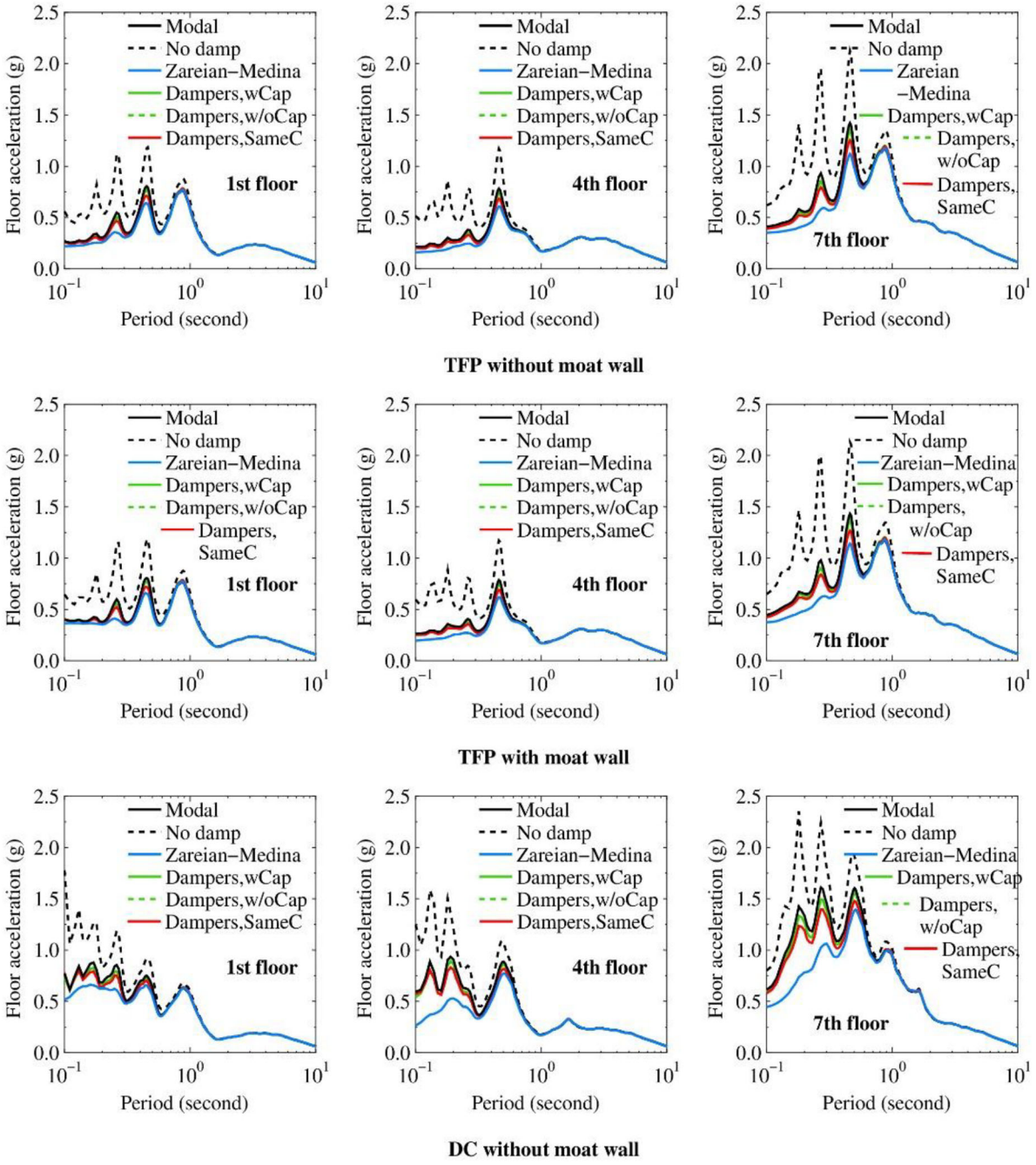

FIGURE 13 Mean floor acceleration spectra of seismically isolated buildings with SMF in 475-year return period round motions

(called "Zareian-Medina"). The seismically isolated building without any inherent damping model was also considered (called "No damp"). All considered inherent damping models were modeled for seismically isolated buildings so that the peak isolator displacement demand was properly calculated without any significant "damping leakage" in isolation system. Two cases of damping value were considered: 0.02 and 0.05 in the second mode.

The assessment of performance was based on the calculation of mean annual frequencies of exceeding specific values of EDPs (peak floor acceleration, peak story drift, peak residual story drift and peak isolator displacement) and on collapse fragility curves constructed using a suite of 400 motions to represent seismic intensities ranging from 43 to 10,000 years of return period for a particular site in California. The collapse fragility curves were then used to compute probabilities of collapse given the MCE_R. The observations of the study, applicable for the two cases of damping value, 0.02 and 0.05, are:

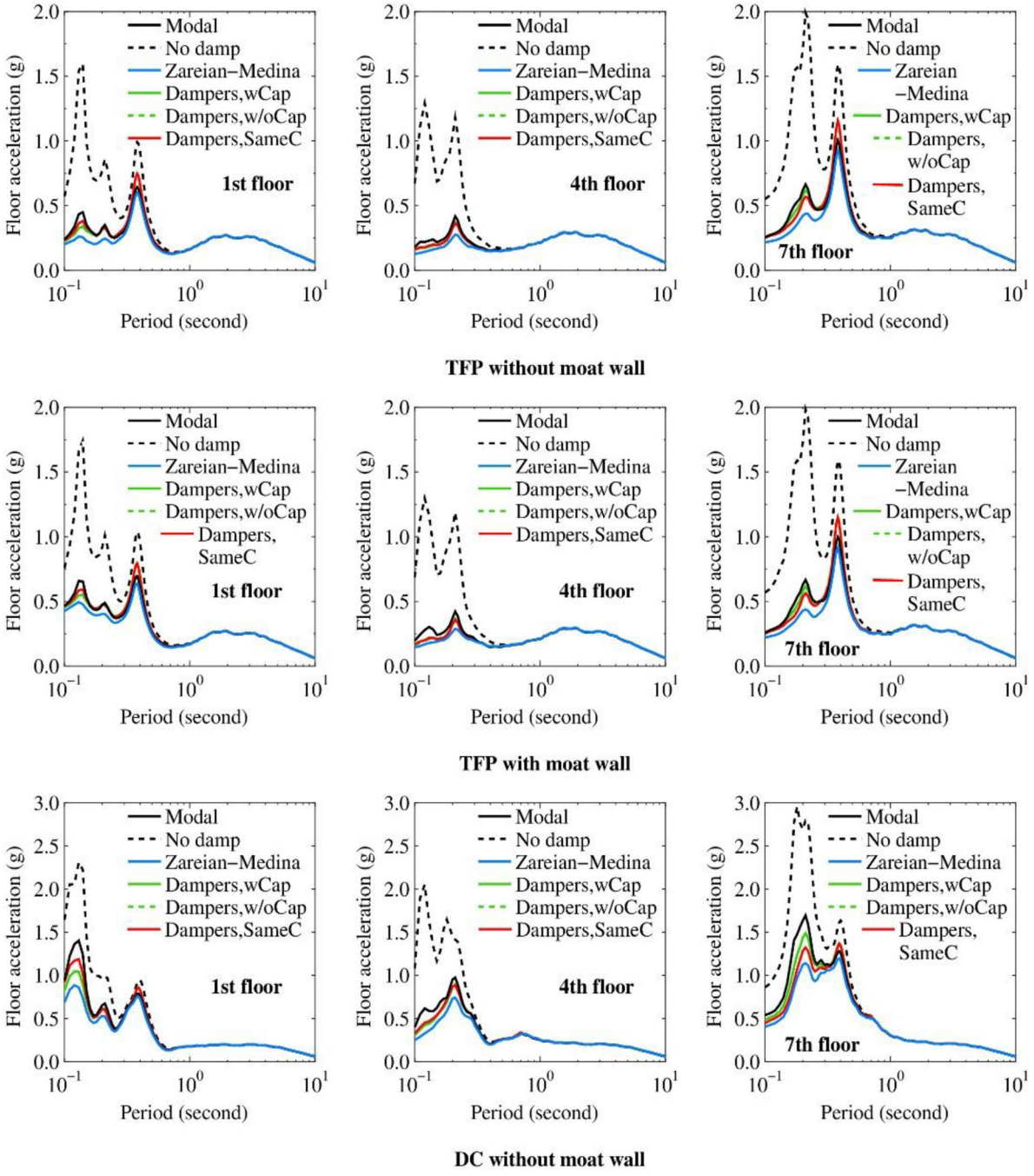

FIGURE 14 Mean floor acceleration spectra of seismically isolated buildings with SCBF in 475-year return period round motions

a. The various inherent damping models considered had insignificant differences in the prediction of the mean annual frequencies of various EDPs, the mean floor response spectra and the probability of collapse given the MCE_R, except for the "Zareian-Medina" model which, for some cases, underpredicted these quantities. This was due to higher values of damping ratio for this model in the higher modes of vibration.
b. Inherent damping needs to be modeled to properly predict responses related to floor peak accelerations and floor spectral accelerations for periods less than about one second. Specifically, specifying zero inherent damping overestimates the peak floor acceleration and the floor response spectra for periods below one second, and underestimates the frequency of occurrence of small/medium values of peak story drift ratio. However, for computing the peak isolator displacement and the collapse probability, use of zero inherent damping does not have any adverse effect on the computed results.

c. The "Dampers,SameC" model in which inherent damping is modeled using virtual linear viscous dampers of the same damping constant without any damper force cap (see Figure 7) was the simplest without the need for complex preliminary calculations (e.g., the "Dampers,wCap", and "Dampers,w/oCap" models require push-over analysis or linear response history analysis) or the use of artificial springs below each isolator for the nonlinear response history analysis. It was also the fastest in terms of execution of nonlinear response history analysis. We recommend its use.

The effect of vertical ground motion on the seismic performance of seismically isolated buildings was not considered in this paper. It is known that the vertical ground motion has insignificant effects on the isolator displacement demands but has some effect on the base shear force and the floor accelerations.[70–72] The effect of using different inherent damping on the seismic performance of seismically isolated buildings considering the effect of vertical ground motions may be worthy of future investigation.

ACKNOWLEDGEMENTS

None.

DATA AVAILABILITY STATEMENT

The data that support the findings of this study are available from the corresponding author upon reasonable request.

ORCID

Shoma Kitayama https://orcid.org/0000-0001-9416-3772

REFERENCES

1. National Institute of Standards and Technology (NIST). Guidelines for nonlinear structural analysis for design of buildings. Part I–General. NIST GCR 17-917-46v1. National Institute of Standards and Technology; 2017. 36p.
2. Grant DN, Diaferia R. Assessing adequacy of spectrum-matched ground motions for response history analysis. *Earthq Eng Struct Dyn*. 2013; 42(9): 1265-1280.
3. National Institute of Standards and Technology (NIST). (2011). Selecting and scaling earthquake ground motions for performing response-history analysis. NIST GCR 11-917-15. National Institute of Standards and Technology; 2011. 256p.
4. Zimmerman RB, Baker JW, Hooper JD, et al. Response history analysis for the design of new buildings in the NEHRP provisions and ASCE/SEI 7 standard: part III—example applications illustrating the recommended methodology. *Earthq Spectra*. 2017; 33(2): 419-447.
5. Ugurhan B, Baker JW, Deierlein GG, Uncertainty estimation in seismic collapse assessment of modern reinforced concrete moment frame buildings. *Tenth U.S. National Conference on Earthquake Engineering. Frontiers of Earthquake Engineering*. July 21–25, 2014. Anchorage, Alaska, USA.
6. Charney FA, Lopez-Garcia D, Hardyniec A, Ugalde D. Modeling inherent damping in nonlinear dynamic analysis. *16th World Conference on Earthquake*. 2017. January 9–13.
7. Luco JE, Lanzi A. A new inherent damping model for inelastic time-history analyses. *Earthq Eng Struct Dyn*. 2017; 46(12): 1919-1939.
8. Bernal D. Viscous damping in inelastic structural response. *J Struct Eng*. 1994; 120(4): 1240-1254.
9. Charney FA. Unintended consequences of modeling damping in structures. *J Struct Eng*. 2008; 134(4): 581-592.
10. Ryan KL, Polanco J. Problems with rayleigh damping in base-isolated buildings. *J Struct Eng*. 2008; 134(11): 1780-1784.
11. Pant DR, Wijeyewickrema AC, ElGawady MA. Appropriate viscous damping for nonlinear time-history analysis of base-isolated reinforced concrete buildings. *Earthq Eng Struct Dyn*. 2013; 42(15): 2321-2339.
12. Sarlis AA, Constantinou MC. *Modeling triple friction pendulum isolators in program SAP2000. Report distributed to the engineering community together with example files*. University at Buffalo, State University of New York; 2010: 55. Available online. Accessed: 6October2022. https://drive.google.com/file/d/1Z5Z7xa5mbZjlXKo-M7YaCYGds2qB5Jnc/view?usp=sharing
13. Giammona AP, Ryan KL, Dao ND. Evaluation of assumptions used in engineering practice to model buildings isolated with triple pendulum isolators in SAP2000. *Earthq Spectra*. 2015; 31(2): 637-660.
14. Anajafi H, Medina RA, Santini-Bell E. Effects of the improper modeling of viscous damping on the first-mode and higher-mode dominated response of base-isolated buildings. *Earthq Eng Struct Dyn*. 2020; 49(1): 51-73.
15. Hall JF. Problems encountered from the use (or misuse) of Rayleigh damping. *Earthq Eng Struct Dyn*. 2006; 35(5): 525-545.
16. Chopra AK, McKenna F. Modeling viscous damping in nonlinear response history analysis of buildings for earthquake excitation. *Earthq Eng Struct Dyn*. 2016; 45(2): 193-211.
17. Hall JF. Performance of viscous damping in inelastic seismic analysis of moment-frame buildings. *Earthq Eng Struct Dyn*. 2018; 47(14): 2756-2776.
18. Heaton TH, Hall JF, Wald DJ, Halling MW. Response of high-rise and base-isolated buildings to a hypothetical mw 7.0 blind thrust earthquake. *Science*. 1995; 267(5195): 206-211.

19. Hall JF, Heaton TH, Halling MW, Wald DJ. Near-source ground motion and its effects on flexible buildings. *Earthq Spectra*. 1995; 11(4): 569-605.
20. Computers and Structures Inc. *SAP2000®: Integrated finite element analysis and design of structures, version 21.2.0, software*. 2019.
21. McKenna FT. *Object-oriented finite element programming: Frameworks for analysis, algorithms and parallel computing*. University of California; 1997: 247p.
22. Kitayama S, Constantinou MC. *Seismic performance assessment of seismically isolated buildings designed by the procedures of ASCE/SEI 7. Report MCEER-18-0004*. Multidisciplinary Center for Earthquake Engineering Research. University at Buffalo, The State University of New York; 2018: 164p.
23. Kitayama S, Constantinou MC. Collapse performance of seismically isolated buildings designed by the procedures of ASCE/SEI 7. *Eng Struct*. 2018; 164: 243-258.
24. Kitayama S, Constantinou MC. Effect of superstructure modeling assumptions on the seismic performance of seismically isolated buildings. *Earthq Eng Struct Dyn*. 2021; 50(7): 1805-1823.
25. Bao Y, Becker TC, Sone T, Hamaguchi H. To limit forces or displacements: collapse study of steel frames isolated by sliding bearings with and without restraining rims. *Soil Dyn Earthq Eng*. 2018; 112: 203-214.
26. Fenz DM, Constantinou MC. Spherical sliding isolation bearings with adaptive behavior: theory. *Earthq Eng Struct Dyn*. 2008; 37(2): 163-183.
27. American Society of Civil Engineers (ASCE). *ASCE/SEI 7–16 Minimum design loads and associated criteria for buildings and other structures*. American Society of Civil Engineers; 2017. 822p.
28. Structural Engineers Association of California (SEAOC). 2012 *IBC SEAOC structural/seismic design manual volume 5: Examples for seismically isolated buildings and buildings with supplemental damping*. Structural Engineers Association of California; 2014. 170p.
29. McVitty WJ, Constantinou MC. *Property modification factors for seismic isolators: design guidance for buildings. Report MCEER-15-0005*. Multidisciplinary Center for Earthquake Engineering Research. University at Buffalo, The State University of New York; 2015: 242p.
30. Ponzo FC, Cesare AD, Leccese G, Nigro D. Shake table testing on restoring capability of double concave friction pendulum seismic isolation systems. *Earthq Eng Struct Dyn*. 2017; 46(14): 2337-2353.
31. British Standards Institution (BSI). *European Standard EN15129: Anti-seismic devices*. British Standards Institution; 2018. 180p.
32. Lee D, Constantinou MC. Combined horizontal-vertical seismic isolation system for high-voltage-power transformers: development, testing and validation. *Bull Earthq Eng*. 2018; 16: 4273-4296.
33. Kitayama S, Constantinou MC. Probabilistic seismic performance assessment of seismically isolated buildings designed by the procedures of ASCE/SEI 7 and other enhanced criteria. *Eng Struct*. 2019; 179: 566-582.
34. Kitayama S, Constantinou MC. Effect of displacement restraint on the collapse performance of seismically isolated buildings. *Bull Earthq Eng*. 2019; 17: 2767-2786.
35. AISC. *Steel construction manual*. AISC; 2017.
36. National Institute of Standards and Technology (NIST). *NEHRP seismic design technical brief No. 4: Nonlinear structural analysis for seismic design: A guide for practicing engineers. NIST GCR 10-917-5*. National Institute of Standards and Technology; 2010.
37. Ibarra LF, Krawinkler H. *Global collapse of frame structures under seismic excitations. Technical Report 152*. John A. Blume Earthquake Engineering Center. Stanford University; 2005: 324p.
38. Eads L. *Seismic collapse risk assessment of buildings: Effects of intensity measure selection and computational approach*. PhD Dissertation. Stanford University; 2013: 357p.
39. Karamanci E, Lignos DG. Computational approach for collapse assessment of concentrically braced frames in seismic regions. *J Struct Eng*. 2014; 140(8): A4014019.
40. Uriz P, Mahin SA. *Toward earthquake-resistant design of concentrically braced steel-frame structures. Technical Report PEER 2008/08*. University of California; 2008: 401p.
41. Lignos DG, Krawinkler H. Deterioration modeling of steel components in support of collapse prediction of steel moment frames under earthquake loading. *J Struct Eng*. 2011; 137(11): 1291-1302.
42. Fenz DM, Constantinou MC. Modeling triple friction pendulum bearing for response-history analysis. *Earthq Spectra*. 2008; 24(4): 1011-1028.
43. Kitayama S, Constantinou MC, Lee D. *Procedures and results of assessment of seismic performance of seismically isolated electrical transformers with due consideration for vertical isolation and vertical ground motion effects*. Multidisciplinary Center for Earthquake Engineering Research. University at Buffalo, The State University of New York; 2016: 180p. *MCEER-16-0010*.
44. Federal Emergency Management Agency (FEMA). *Quantification of building seismic performance factors. Report FEMA P695*. Federal Emergency Management Agency; 2009. 422p.
45. Pant DR, Wijeyewickrema AC. Structural performance of a base-isolated reinforced concrete building subjected to seismic pounding. *Earthq Eng Struct Dyn*. 2012; 41(12): 1709-1716.
46. Hughes PJ, Mosqueda G. Evaluation of uniaxial contact models for moat wall pounding simulations. *Earthq Eng Struct Dyn*. 2020; 49(12): 1197-1215.
47. Wilson EL, Penzien J. Evaluation of orthogonal damping matrices. *Numer Methods Eng*. 1972; 4(1): 5-10.
48. Chopra AK. *Dynamics of structures: Theory and applications to earthquake engineering*. 5thed. 2020: 992p.
49. Qian X, Chopra AK, McKenna F. *Modeling viscous damping in nonlinear response history analysis of steel moment-frame buildings: Design-plus ground motions. Revision 1.0. PEER 2020/01*. Pacific Earthquake Engineering Research Center. University of California, Berkeley; 2020: 143p.

50. Ramirez OM, Constantinou MC, Kircher CA, et al. *Development and evaluation of simplified procedures for analysis and design of buildings with passive energy dissipation systems*. Multidisciplinary Center for Earthquake Engineering Research. University at Buffalo, The State University of New York; 2001: 510p. *Report MCEER-00-0010*.
51. Akcelyan S, Lignos D, Hikino T. Adaptive numerical method algorithms for nonlinear viscous and bilinear oil damper models subjected to dynamic loading. *Soil Dyn Earthq Eng*. 2018; 113: 488-502.
52. Zareian F, Medina RA. A practical method for proper modeling of structural damping in inelastic plane structural systems. *Comput Struct*. 2010; 88(1-2): 45-53.
53. Federal Emergency Management Agency (FEMA). Seismic performance assessment of buildings. Report FEMA P-58. Volume 1 – Methodology. Second Edition. Federal Emergency Management Agency; 2018. 340p.
54. Lin T, Haselton CB, Baker JW. Conditional spectrum-based ground motion selection. Part I: hazard consistency for risk-based assessments. *Earthq Eng Struct Dyn*. 2013; 42(12): 1847-1865.
55. Jalayer F. *Direct probabilistic seismic analysis: Implementing non-linear dynamic assessments*. Stanford University: 243p.
56. Baker JW. Conditional mean spectrum: tool for ground-motion selection. *J Struct Eng*. 2011; 137(3): 322-331.
57. Kitayama S, Constantinou MC, "Effect of modeling of inherent damping on the response and collapse performance of seismically isolated buildings — Digital Appendix" 2022. 63p. (Accessed:8October2022) Available online: https://drive.google.com/file/d/1NNVbhrALwNeyWfLcU7hD3ghYUJu0Ypj/view?usp=sharing
58. Shinozuka M, Feng MQ, Lee J, Naganuma T. Statistical analysis of fragility curves. *J Eng Mech*. 2000; 126(12): 1224-1231.
59. Baker JW. Efficient analytical fragility function fitting using dynamic structural analysis. *Earthq Spectra*. 2015; 31(1): 579-599.
60. Sabelli R, Roeder CW, Hajjar JF. *Seismic design of steel special concentrically braced frame systems – A guide for practicing engineers. NEHRP Seismic Design Technical Brief No. 8, NIST GCR 13-917-24*. National Institute of Standards and Technology; 2013: 36p.
61. Federal Emergency Management Agency (FEMA). *NEHRP guidelines for the seismic rehabilitation of buildings. Report FEMA 273*. Federal Emergency Management Agency; 1997. 435p.
62. Bernal D, Döhler M, Kojidi SM, Kwan K, Liu Y. First mode damping ratios for buildings. *Earthq Spectra*. 2015; 31(1): 367-381.
63. Masroor A, Mosqueda G. Assessing the collapse probability of base-isolated buildings considering pounding to moat walls using the FEMA P695 methodology. *Earthq Spectra*. 2015; 31(4): 2069-2086.
64. Pavlou E, Constantinou MC. Response of nonstructural components in structures with damping systems. *J Struct Eng*. 2006; 132(7): 1108-1117.
65. Miranda E, Taghavi S, A comprehensive study of floor acceleration demands in multi-story buildings. *ATC and SEI Conference on Improving the Seismic Performance of Existing Buildings and Other Structures*. December 9–11, 2009.
66. Wolff ED, Ipek C, Constantinou MC, Tapan M. Effect of viscous damping devices on the response of seismically isolated structures. *Earthq Eng Struct Dyn*. 2015; 44(2): 185-198.
67. Vukobratović V, Fajfar P. A method for the direct estimation of floor acceleration spectra for elastic and inelastic MDOF structures. *Earthq Eng Struct Dyn*. 2016; 45(15): 2495-2511.
68. Anajafi H, Medina RA. Evaluation of ASCE 7 equations for designing acceleration-sensitive nonstructural components using data from instrumented buildings. *Earthq Eng Struct Dyn*. 2018; 47(4): 1075-1094.
69. Molina Hutt C, Almufti I, Willford M, Deierlein D. Seismic loss and downtime assessment of existing tall steel-framed buildings and strategies for increased resilience. *J Struct Eng*. 2016; 142(8): C4015005.
70. Sarlis AA, Constantinou MC, Reinhorn AM. *Shake Table Testing of Triple Friction Pendulum Isolators under Extreme Conditions. Report MCEER-13-0011*. Multidisciplinary Center for Earthquake Engineering Research. University at Buffalo, The State University of New York; 2013: 450p.
71. Ryan KL, Dao ND. Influence of vertical ground shaking on horizontal response of seismically isolated buildings with friction bearings. *J Struct Eng*. 2016; 142(1): 04015089.
72. Cilsalar H, Constantinou MC. Effect of vertical ground motion on the response of structures isolated with friction pendulum isolators. *Int J Earthq Impact Eng*. 2017; 2(2): 135-157.

SUPPORTING INFORMATION

Additional supporting information can be found online in the Supporting Information section at the end of this article.

How to cite this article: Kitayama S, Constantinou MC. Effect of modeling of inherent damping on the response and collapse performance of seismically isolated buildings. *Earthquake Engng Struct Dyn*. 2023;52:571–592. https://doi.org/10.1002/eqe.3773